Hydrodynamics and water properties at the entrance of Araçá Bay, Brazil

Marcelo Dottori [1] · **Eduardo Siegle** [1] · **Belmiro Mendes Castro** [1]

Abstract Current meter and hydrographic properties at the entrance of the Araçá Bay (AB), an intertidal flat adjacent to the São Sebastião channel, were collected between July 2013 and February 2014. These data sets show two different hydrographic periods, marked by a sharp change in the temperature and salinity values, clearly caused by the arrival of the South Atlantic Central Water (SACW). The first period is characterized by small variabilities on both properties with the dominance of coastal water, with relatively low salinity values. The second period shows a strong increase in the average salinity values and a much larger variability of temperature. This change in the hydrographic characteristics seems to be caused by anomalous winds, capable of displacing the SACW toward the coast. On the other hand, current meter data shows that the dynamics is mainly driven by the large-scale wind and is not impacted by the arrival of the SACW. Also, the currents are dominated by the barotropic mode, independently of the stratification differences that are observed between the beginning and end of the observational period.

Responsible Editor: Arnoldo Valle-Levinson

This article is part of the Topical Collection on *Physics of Estuaries and Coastal Seas 2014 in Porto de Galinhas, PE, Brazil, 19-23 October 2014*

✉ Marcelo Dottori
   mdottori@usp.br

[1] Oceanographic Institute, University of São Paulo, Praça do Oceanográfico 191, 05508-120 São Paulo, SP, Brazil

1 Introduction

The South Brazil Bight (SBB, Fig. 1), located between the Cape of Santa Marta and Cabo Frio, has a shelf relatively wide in its central part, reaching about 200 km, but it narrows on the southern and northern parts, reducing to about half of that distance. The shelf break occurs at depths up to 180 m, with the Brazil Current flowing at the slope.

In terms of dynamics, the central part of the SBB can be partitioned into three regions: the inner, the middle, and the outer shelf (Castro et al. 1987; Castro 1996). The currents in the inner shelf are mainly dominated by the synoptic wind regime and by a line source of freshwater discharged by many small and medium estuarine systems (Castro 1996; Castro et al. 2008). The middle shelf responds basically to the wind regime (Dottori and Castro 2009) and the outer shelf to the wind and the constant intrusions of the Brazil Current (Castro 1996).

The winds in the region are associated to the South Atlantic High, blowing from east-northeast, leaving the coast to the right in the SBB, and the passage of cold front systems, which happens during the whole year, with winds blowing from the south, leaving the coast to the left. The forced coastal jets (Csanady 1977) have the same direction as the forcing wind stress (Dottori and Castro 2009). The thermohaline currents, on the other hand, do not change its direction, leaving the coast to the left in the SBB due to geostrophic constraints (McClimans 1986).

Regarding the termohaline properties, the SBB is filled by three water masses and by the products of their mixing (Castro and Miranda 1998; Castro 2014; Cerda and Castro 2013): the nearshore coastal water (CW), relatively fresh and warm; the outer shelf surface tropical water (TW), relatively warm ($T >$ 20 °C; T is temperature) and salty ($S > 36$, S is salinity) (Emilsson 1961); and the outer shelf bottom South Atlantic
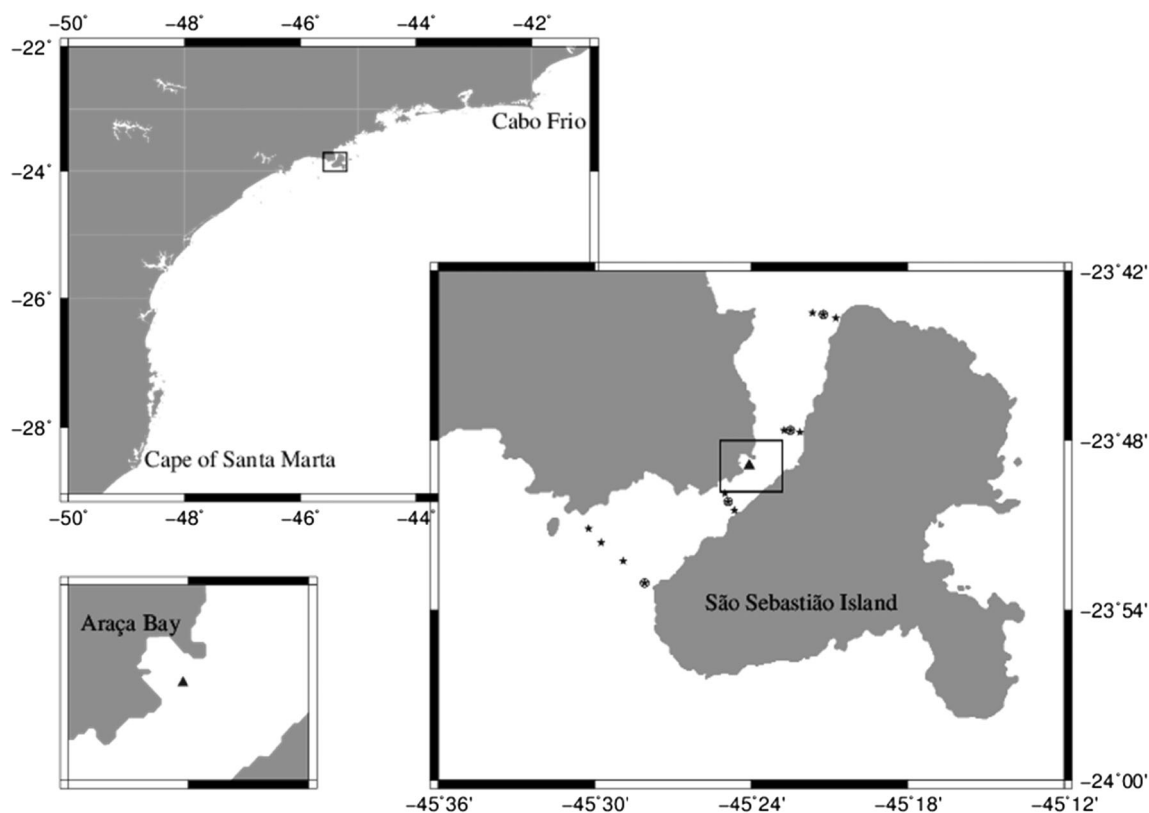
Fig. 1 The São Sebastião Island and the location of the mooring (*triangle*) and the hydrographic stations (*stars*) in the São Sebastião Channel. The hydrographic stations marked also with a *circle* represent the deepest point of the transect. The Araçá Bay, located in the continental margin of the São Sebastião Channel, is shown in more details at the *bottom left corner*, with the location of the mooring (*triangle*) at its entrance. *Top left pannel* shows the South Brazil Bight

Central Water (SACW), colder than the other two (T<18 °C) and with salinities between 35 and 36. The SACW covers the bottom layer of the SBB between the continental shelf break (180 m depth) and the 70–100-m isobath (Castro 2014). This last water mass surfaces in the northern SBB during coastal upwelling, mainly in the Cabo Frio region, and makes the SBB middle shelf highly stratified due to its presence bellow the pycnocline (Castro 2014).

The São Sebastião Channel (SSC), located in the central part of the SBB and, most of the time, in the inner shelf, runs between the continent and the Island of São Sebastião (Fig. 1). Therefore, the currents in the SSC are dominated by the wind and termohaline forcings, with weak tidal currents due to the almost stationary tidal wave generated within the channel when the tidal wave reaches its extremities almost simultaneously (Castro 1990). Tidal currents have some importance in the cross-shore direction both in the SSC and in the SBB. However, the cross-shore variability is at least 1 order of magnitude smaller than variability in the alongshelf direction (Dottori and Castro 2009). During persistent upwelling favorable wind events, especially during summer and spring, numerical experiments show that the SACW can intrude into the of SSC (Coelho 1997).

Influenced by the hydrodynamics and water properties in the area is the adjacent Araçá Bay (AB), one of few tide-dominated environments along the southeastern coast of Brazil. This bay is relatively small (approximately 750 m wide and 750 m long) and protected from the incident swell by the large São Sebastião island, approximately 28 km long. The Araçá Bay is located in the continental side of the São Sebastião Channel (Fig. 1), and according to the classification proposed by Dyer et al. (2000), it is a mid-latitude tidal flat of temperate region.

The Araçá Bay has a large marine biodiversity (Amaral et al. 2010) and can be classified, according to Dionne (1988), as a wet subtropical flat colonized by mangroves. This bay has been intensively modified during the last decades, with land reclamation due to harbor construction reducing its size drastically by one third since 1973 (Villamarin 2014). The data used in this study was collected at the entrance of this intertidal flat, and our findings are relevant to this intertidal area since the biogeochemical and termohaline properties of the incoming waters during flood are highly important for the biological processes in those diverse areas.

In this work, we address the forcing mechanisms and the associated hydrodynamic response, including the water mass characteristics at a shallow area at the entrance of the Araçá Bay. We use data collected during approximately 6 months in the region for verifying whether or not the synoptic winds drive a portion of the variability observed in this small and very peculiar environment, besides the tides.

2 Data and methods

2.1 Data set

A mooring instrumented with two conductivity and temperature (CTs) and an acoustic doppler current profiler (ADCP) operated in the entrance of the AB from August 2013 to February 2014, totaling 6 months of almost continuous

Fig. 2 Raw time series of salinity (*top panel*) and temperature (*bottom panel*) after the removal of spurious values. The initial time is August 1, 2013 at 00:00 h
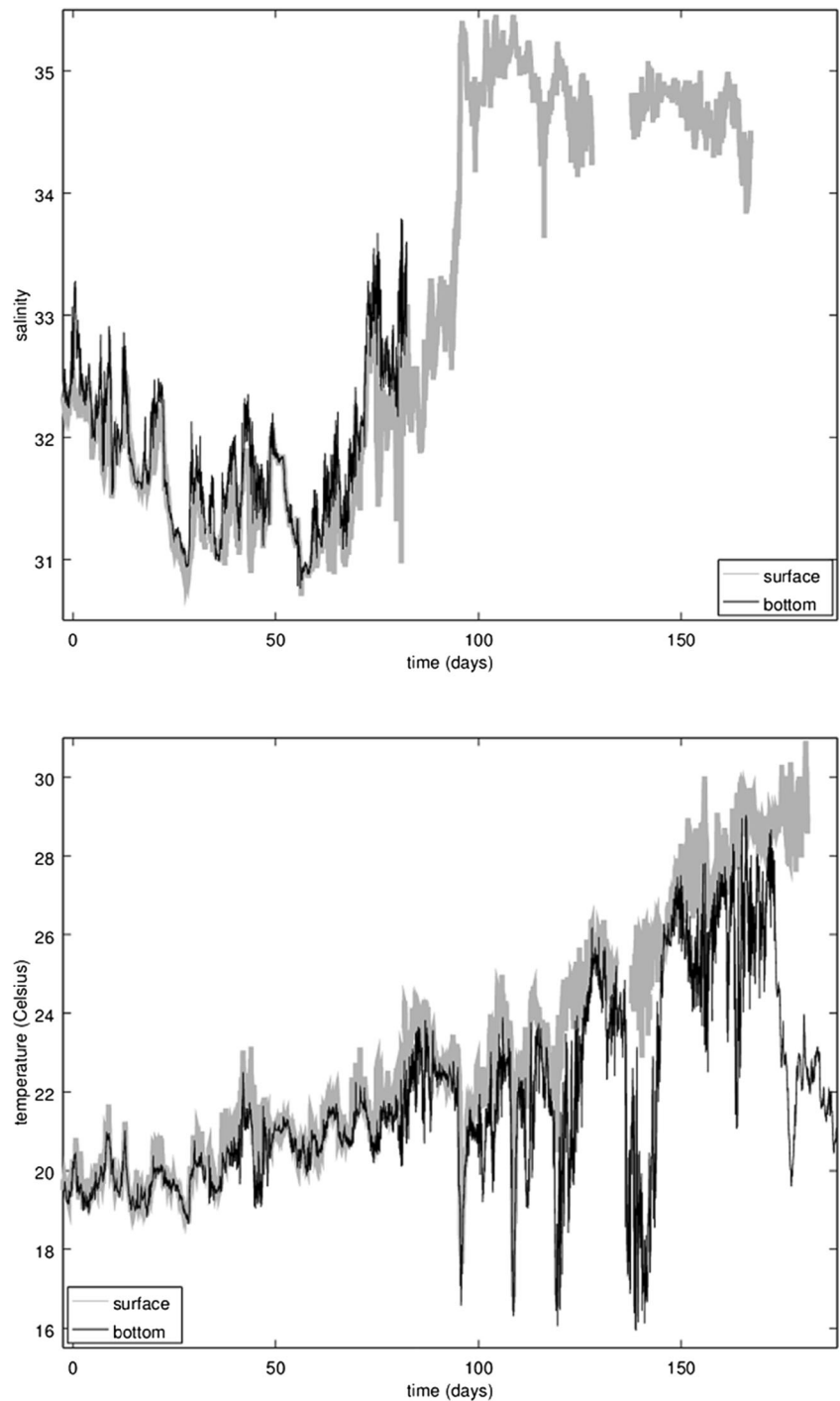
Table 1 Main statistical parameters for the temperature and salinity time series

Region	Temperature (°C–°C/month)		Salinity (dimensionless–1/month)	
	Surface	Bottom	Surface	Bottom
Mean total	23.11	21.78	32.97	–
Mean 1st period	20.89	20.54	31.75	31.88
Mean 2nd period	25.56	22.97	34.72	–
Trend total	1.63	0.84	0.78	–
Trend 1st period	1.11	0.29	0.10	0.016
Trend 2nd period	2.90	1.22	-0.04	–

The first period comprehends the first 95 days and the second from day 96 to the end of the records. Salinity at the bottom, however, comprehends only the first 85 days of the records

measurements. Sampling rate was 0.5 hour in the first month and 1.0 hour for the rest of the experiment. The CT precision was ±0.01 for both temperature and salinity, and they were located at 1 m below the sea surface and near to the bottom (≈10 m). The ADCP was deployed near to the bottom and measured currents every meter up to the sea surface. Maintenance cruises were realized every 2 to 3 months.

Hydrographic data from 13 oceanographic stations covering the SSC from south to north (Fig. 1), collected during 8-h cruises realized in October and December of 2013 and in March of 2014, were also used. The data set consists of vertical profiles of temperature and salinity every meter, from the surface to the bottom. The instrument used in the hydrographic cruises was a CastAway-CTD, from Sontek/YSI, with precision of 0.1 for salinity and 0.05 °C for temperature.

Surface winds from the NCEP Reanalysis 2 (Kanamitsu et al. 2002), recorded every 6 h at 42.5° W, 25° S, were also used.

2.2 Methods

The temperature and salinity time series had spikes removed using a ±1 standard deviation criterion followed by linear interpolations to substitute for the removed values. Bottom salinity records presented some inconsistencies, causing the bottom density being smaller than the surface density. In this case, the bottom salinity record was removed (about 50 % of the values were removed). The surface salinity time series had also about 10 days of data removed due to a malfunctioning of the sensor. The processed temperature and salinity time series are shown in Fig. 2.

The other data sets were also inspected visually and checked for anomalous extreme values. For the three SSC hydrographic cruises and for the NCEP winds, it was not necessary to remove any data.

Power spectra for the T and S time series were computed using the Welch (1967) method, after removing the linear

Fig. 3 TS diagram for the whole period. The *lighter dots* show temperature/salinity pairs for the first period. The *darker dots* show the temperature/salinity pairs for the second period. The *horizontal line* shows the 18 °C isotherm, and the vertical line the 34 isohaline
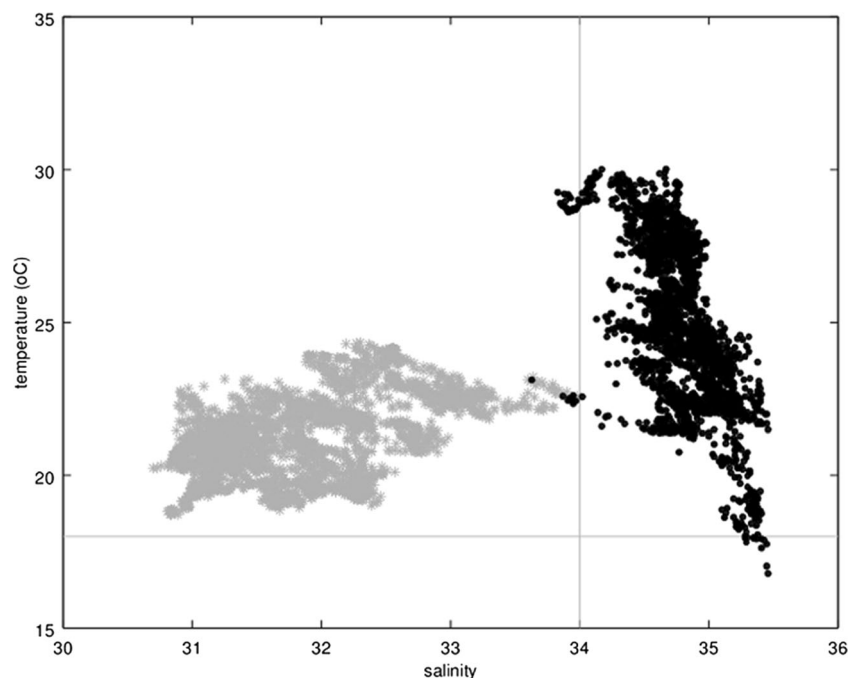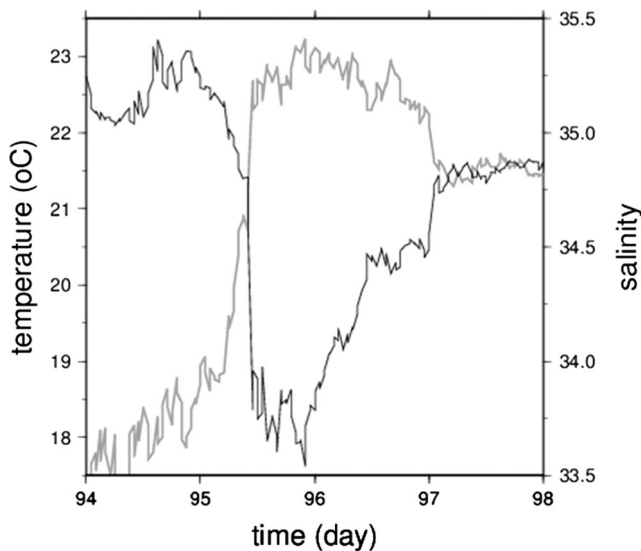
Fig. 4 Surface temperature (*dark line*) and salinity (*gray line*) time series around day 95 of the experiments. Changes on both values are very sharp and occur simultaneously

trend and the mean from the time series. A 2-month window with 50 % of overlap was used in this analysis, and gaps in the time series were filled with zeros.

Linear trends for the *T* and *S* time series were estimated for the whole, first half (from day 1 to day 95), and second half of the series (from day 95 to the end). This analysis was performed due to the distinct behavior of the time series for each period, as can be noticed in Fig. 2.

Lagged correlation coefficients were estimated between the *T* and *S* time series and the alongshore and cross-shore components of the wind and of the wind stress. The lagged

correlations were also estimated for the whole, first half, and second half of the time series, after removing the mean and linear trend. An angle of 50° from the real north, in the clockwise direction, was used to decompose the wind and the current vectors in their alongshore and cross-shore components.

Low-passed time series were generated using a 40-h Lanczos squared filter in order to remove the suprainertial frequencies (inertial period in the SSC is about 29.7 h).

A complex empirical orthogonal function (EOF) analysis was performed for both the ADCP current time series: raw and low-passed.

3 Results

A visual analysis of the *T* and *S* time series (Fig. 2) shows different time behaviors for those fields. *T* records, both at the surface and at the bottom, have a first period, up to day 95, of relatively small variability and slow increase, followed by a period of strong temperature variability and increase in the linear trend (Table 1). While in the first period, *T* varies between 19 and 23 °C, in the second period, the temperatures oscillate between 16 and 30 °C. Salinities oscillate between 1 and 2 units around the mean in both periods, with relatively smooth linear trends in each one of the two periods (Table 1). There is an abrupt change in *S* near the day 95. This jump in surface *S* was used to separate the *T* and *S* time series in the two periods already mentioned. The TS diagram (Fig. 3) also shows the clear jump from the first to the second period, highlighted in Fig. 4. Figures 2.4 and 2.5 (left panels) of Castro et al. (2008) show almost no variability of *T* and *S* in

Fig. 5 The bars show the monthly average cross-shore (*top*) and alongshore (*bottom*) components of wind at 42.5° W and 25° S, from NCEP–NCAR, between 1990 and 2012. The *gray lines* show the monthly averages between August 2013 and February 2014. Negative values of the alongshore component favors the intrusion of the SACW and are clearly more intense in the months of November of 2013 and January and February of 2014
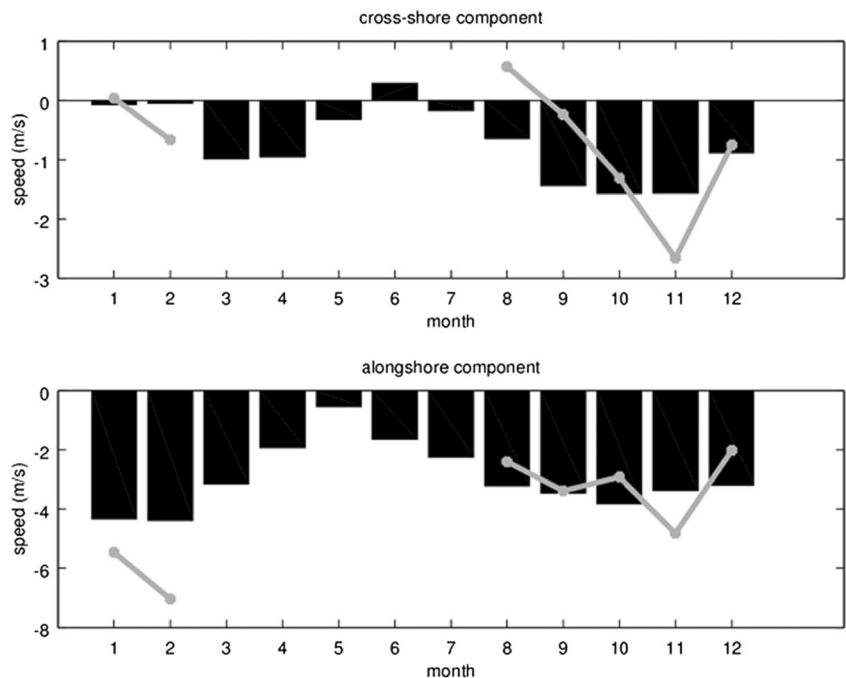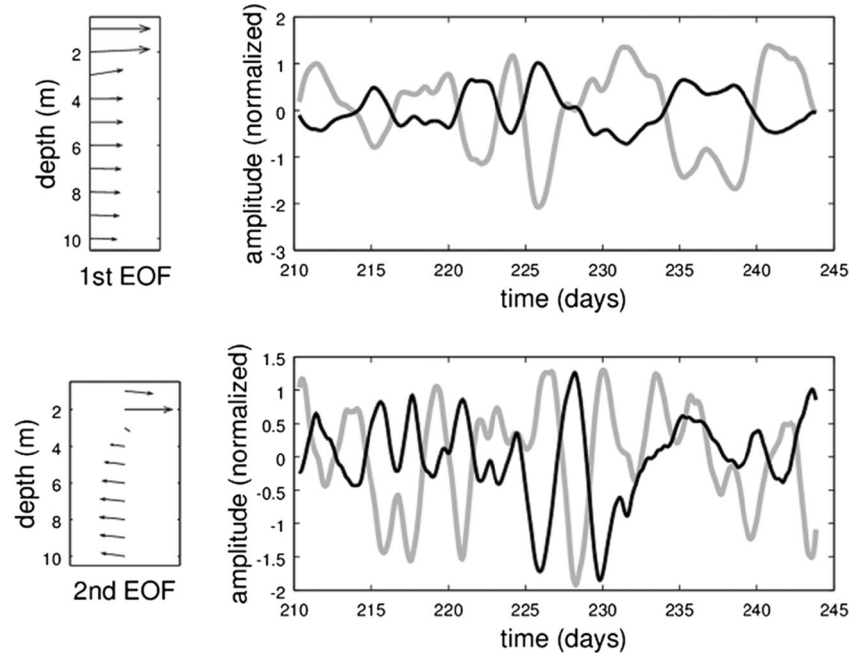
Fig. 6 The vertical structure of the EOFs IS presented on the *left panels* and, on the *right*, the principal components. The first EOF, corresponding to the barotropic mode, is on the *top*, and the second EOF, corresponding to the first baroclinic mode, is on the *bottom*. These results were obtained with the ADCP data set between July 25 and September 2 of 2013

the SSC during the austral winter of 1992 and 1993 and, during the summer of the same years, a much larger variability. In fact, temperature and salinity values associated with the SACW are observed in the SSC only during the summer years, but only at the bottom of the channel.

Temperatures showed a smaller mean vertical gradient in the first period, when the mean surface and bottom T was 20.89 and 20.54 °C, respectively, than in the second period, when mean surface and bottom T was 25.56 and 22.97 °C, respectively (Table 1). The lower stratification in the first

period is also confirmed by the small vertical variability in S: 31.75 at surface and 31.88 at bottom (Table 1).

Power spectra calculated for the T and S time series (not shown) indicate that most of the variability is found in the subinertial band. Energy peaks were found for both T time series at periods of 10.5 days and its harmonics, and 1 day, the first period having higher energy; for the bottom S time series, there was a peak at 8.3 days. The wind time series also has the main variability associated with the subinertial band. Energy peaks in the spectra were observed for the 10.5, 7, 6, and 4.4 days, approximately.

Fig. 7 The vertical structure of the EOFs is presented on the *left panels* and, on the *right*, the principal components. The first EOF, corresponding to the barotropic mode, is on the *top* and, the second EOF, corresponding to the first baroclinic mode, is on the *bottom*. These results were obtained with the ADCP data set between September 2 and October 21 of 2013
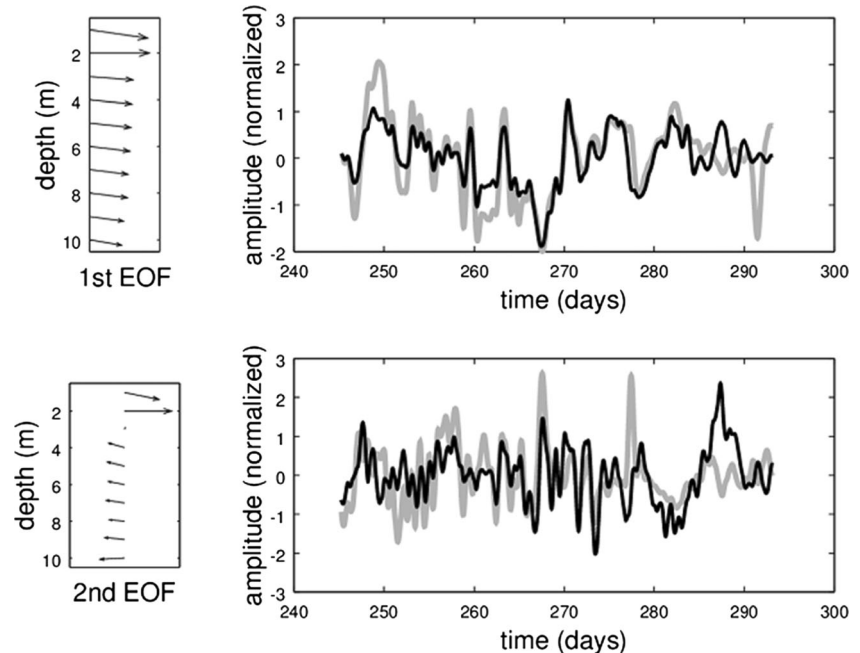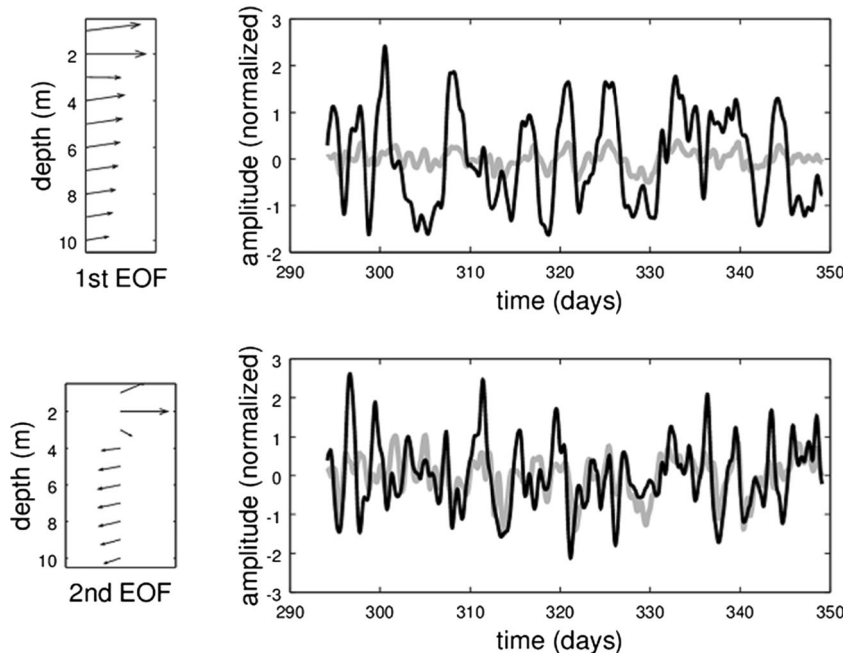
Fig. 8 The vertical structure of the EOFs are presented on the *left* panels and, on the right, the principal components. The first EOF, corresponding to the barotropic mode, is on the *top* and, the second EOF, corresponding to the first baroclinic mode, is on the *bottom*. These results were obtained with the ADCP data set between October 21 and December 16 of 2013

Lagged correlation coefficients between the wind/wind stress and the T and S time series are statistically significant only for the second half of the series, after day 95. For the surface T, the correlation with the cross-shore wind stress is 0.59, above the 99 % significance level, and with a delay of 62 h, wind stress leading. Correlations between surface T and the alongshore wind stress did not reach the 95 % significance level. At the bottom, the lagged correlation coefficients between T and cross-shore wind stress and alongshore wind stress reached 0.46 and 0.44, respectively, with a delay of 104 and 29 h, wind leading. All these results are above the 99 % significance level.

For surface S, the lagged correlation coefficient with the cross-shore wind stress for the second period is 0.57, with a delay of 96 h, above the 99 % confidence level.

The hydrographic cruises in SSC were used, mainly, to map the occurrence of SACW. The profiles from October 2013 (not shown) present waters relatively warm, above 19 °C. Only in the cruise from December 2013 (Fig. 11) is possible to observe water temperatures below 18 °C, showing the presence of the SACW.

Calculations for the monthly mean calculated using 23 years of the NCEP winds (from 1990 to 2013) show that the mean alongshore component is negative throughout the year, but more intense during the austral spring and summer months (Fig. 5). It is also possible to notice in Fig. 5 that the end of spring and the summer months of the year 2013 presented winds more intense than the 23-year monthly means.

EOFs for the current meter time series were also calculated for the three periods between maintenance of the mooring. In all cases (Figs. 6, 7, and 8 and Table 2), there are two main dynamical modes clearly identified, the barotropic and the first baroclinic. The barotropic mode dominates all time series,

responding for at least 79 % of the variability in the raw records and, after low-pass filtering, at least 88 %. The first baroclinic mode responds for no more than 14 % of the variability in the raw time series and 9 % in the low-passed time series.

Correlation between the first complex principal component, associated with the barotropic mode, and the wind stress were estimated, for both real and imaginary parts and both components of the wind stress. The results (Table 3) consistently show a dynamic response of the water to the wind stress. For the raw time series, the highest correlation coefficient values are approximately 0.6, while for the filtered time series, the highest values are approximately 0.8, showing that subinertial current variability is largely driven by the wind stress oscillations. Note that, differently from TS time series, the current meter records did not follow the same partitioning. In fact, during the whole period, currents show the same characteristics in terms of dynamics and are strongly associated with the large-scale wind stress.

Table 2 Contribution of the first two EOFs to the current meter variability, for both raw and low-pass filter time series

	1st EOF		2nd EOF	
Period (in 2013)	Raw	Filtered	Raw	Filtered
July 25 to September 2	87 %	97 %	8 %	2.7 %
September 2 to October 21	79 %	88 %	10 %	7 %
October 21 to December 16	79 %	90 %	14 %	9 %

Note that the first EOF corresponds to the barotropic mode and the second EOF to the first baroclinic (Figs. 6, 7, and 8)

EOF empirical orthogonal function

Table 3 Lag correlation coefficient between the cross-shore and alongshore components of the wind and the real and imaginary part of the first principal component obtained with the complex EOF analysis

		Raw		Filtered	
Period	Wind component	Real	Imaginary	Real	Imaginary
July 25 to September 2	Cross-shore	0.54 (−13 h)	−0.57 (−27 h)	0.76 (−23 h)	−0.72 (−24 h)
	Alongshore	0.61 (12 h)	−0.70 (12 h)	0.78 (16 h)	−0.82 (15 h)
September 2 to October 21	Cross-shore	−0.45 (−64 h)	−0.49 (−64 h)	−0.60 (−37 h)	−0.65 (−49 h)
	Alongshore	−0.54 (11 h)	0.46 (11 h)	−0.62 (11 h)	−0.52 (10 h)
October 21 to December 16	Cross-shore	0.66 (−45 h)	0.28 (−38 h)	0.78 (−41)	0.54 (−48 h)
	Alongshore	0.60 (18 h)	0.27 (29 h)	0.66 (20 h)	0.49 (21 h)

4 Discussion and final remarks

At the entrance of the Araçá Bay, current and hydrographic properties are strongly influenced by the synoptic wind. Subinertial current variability, besides being the most energetic, shows high correlation with the wind stress. Subinertial temperature and salinity variability show higher correlation with the wind stress during the second sampling period. So why did the wind force temperature and salinity variations mostly during the second sampling period while the same winds forced current variability during the whole experiment time?

Initially, currents respond to wind stress forcing almost instantaneously or with a lag in time, depending on the type of response being highly or poorly influenced by bottom friction. In the first case, the response is almost instantaneous and in the form of arrested topographic waves (Csanady 1978); when bottom friction has a smaller order, the lag in time response can be in the form of continental shelf waves (Gill and Schumann 1974; Clarke and Brink 1985). There are several authors who showed that the response of the SBB waters to the wind stress happens preferentially in the form of continental shelf waves and it is better correlated with winds that happened earlier in time and southward from the local of observation (Castro and Lee 1995; Campos et al. 2000). Nevertheless, the almost in-phase response to the local wind cannot be neglected in the SBB as showed by several authors (Stech and Lorenzzetti 1992; Dottori and Castro 2009). Within the SSC, Castro (1990) showed that the current response to the wind stress forcing is not only locally forced, attributing part of the observed variance to remotely forced continental shelf waves. Those previous works show that the currents in the SBB and within the SSC are mainly forced by the wind stress, either local or remote. That is the reason why we have found in this paper high correlations between the low-passed currents and winds, both for the real current time series and for the first principal component (barotropic) current time series.

Fig. 9 TS diagram of all hydrographic stations in the SSC (Fig. 1) collected in July 30 2013
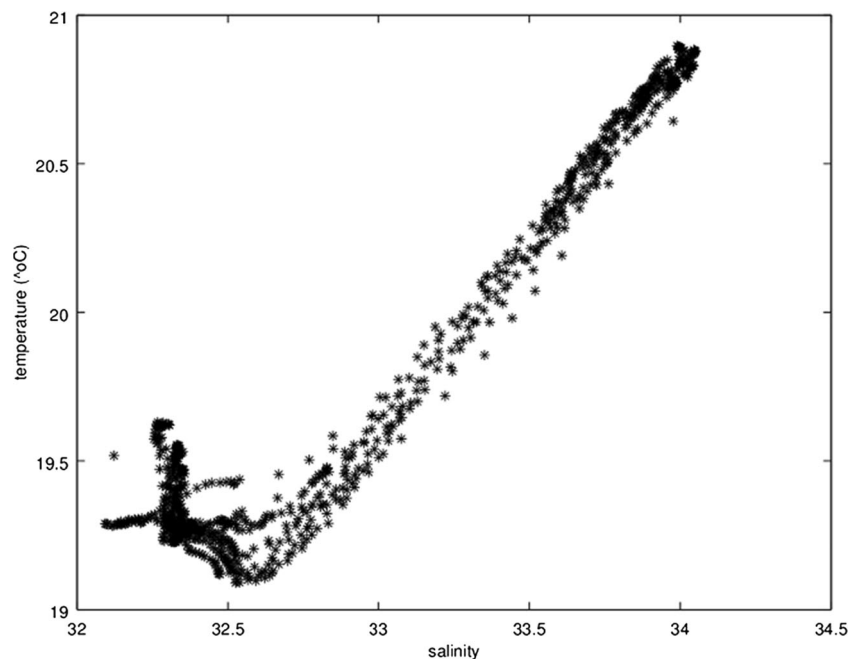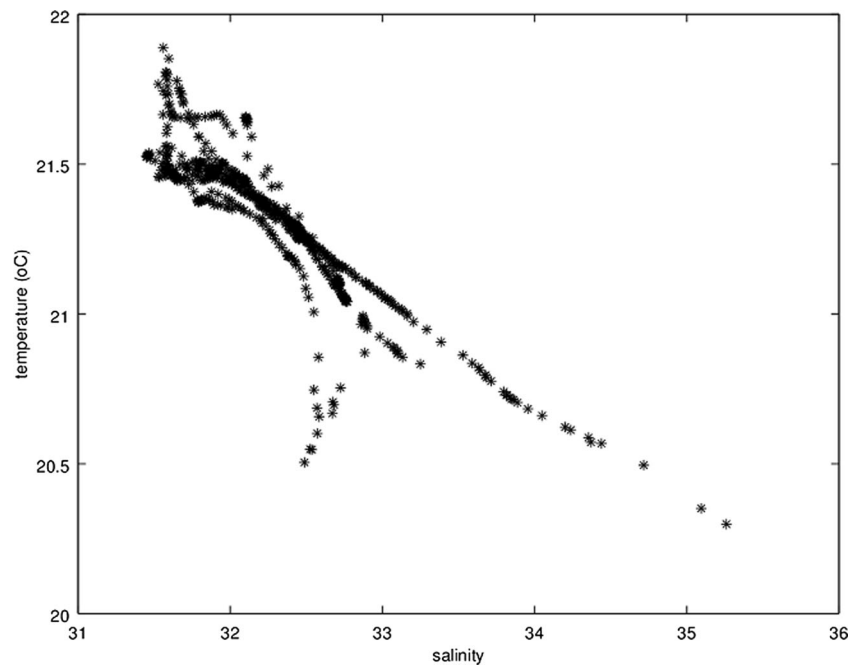
Fig. 10 TS diagram of all hydrographic stations in the SSC (Fig. 1) collected in October 4 2013


Castro (2014) showed that the vertical stratification in the SBB coastal region increases only if there is buoyancy advection from low-salinity inner shelf waters or from SACW intruding toward the coast. During the first half of the observations, the TS diagram (Fig. 3) showed a predominance of CW, with relatively high temperatures and low salinities, and it is very clear that temperature varied little in the vertical and never reached values below 18 °C, the threshold for the SACW. Also, salinity values are below 34, usually below

33, indicating the dominance of the CW. Therefore, during the first period, temperature and salinity vertical gradients are small and almost steady, showing that T and S oscillations due to the advection are not a strong feature because there was no advection of either low-salinity waters or of SACW.

Approximately at day 95, however, there is a sharp decrease in temperature and a sharp increase in salinity (Fig. 4), showing the advection of the SACW toward the entrance of the AB. It is the advection of this water mass that

Fig. 11 Vertical profiles of temperature at the deepest station of each transect shown in Fig. 1. The profiles are ordered from south (*left panel*) to north (*right panel*) and were obtained on December 3, 2013
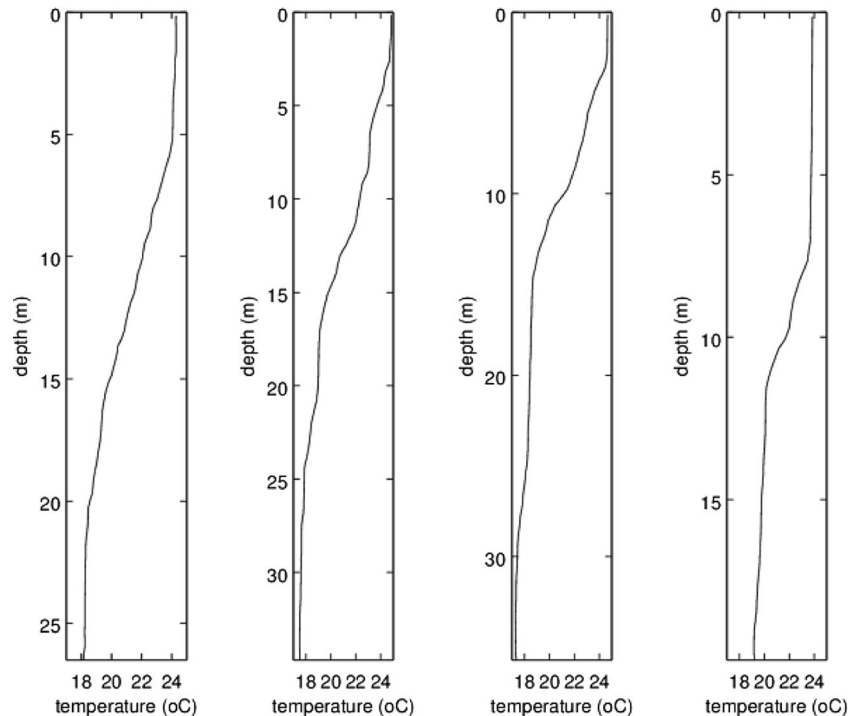
changed how *T* and *S* respond to the synoptic winds. Since the vertical stratification is linked to the buoyancy advection of the SACW, and since this advection is due to the wind stress variability, there is a higher correlation between the *T* and *S* fields and the wind stress during the second observation period. In this second half, the TS diagram consistently changes format (Fig. 3), indicating the influence of the cold SACW. Other authors had already detected the presence of the SACW in the SSC, both in observations (Coelho 1997; Castro and Miranda 1998; Castro et al. 2008) and in numerical experiments (Silva et al. 2005).

Additional support for the partitioning of the sampling period in two parts, with different hydrothermodynamic properties in each one, is brought by the hydrographic data from the oceanographic cruises. *T* and *S* from the cruises that took place in July and in October of 2013 do not show the presence of the SACW in the SSC (Figs. 9 and 10), since all the temperatures are above 19 °C. These two cruises were realized before day 95 of the mooring time series collected at the entrance of AB. Data from the December 2013 cruise, however, show temperatures below 18 °C, demonstrating the presence of the SACW in the region, as demonstrated in Fig. 11, containing the vertical temperature profiles for the deepest station at each transect (see Fig. 1). This last cruise was realized within the second half of the time series, after day 95, when the temperature variability is large and the SACW was observed at the entrance of the AB.

Due to its high density, the SACW is observed most frequently in the bottom layer of the SSC, especially in the deepest region that runs along the insular side of the channel. In the second measurement period, the SACW was observed at the entrance of the AB, from the bottom to near surface (Fig. 2). This anomalous location of the SACW was due to the anomalous winds observed in the summer months, as shown in Fig. 5. The normal year average summer winds already favor intrusions of the SACW into the SSC, but during the austral summer of 2013/2014, the intrusion favorable winds were more frequent and intense, moving the SACW toward the surface and along the SSC.

Although the changes in salinity and temperature in the SSC might take some time to develop, locally, at the entrance of AB, the process is fast and takes a few hours to occur. In 24 h, at day 95, temperature dropped more than 5 °C and salinity increased almost 2 units (Fig. 4). This leaves no doubt that, in fact, it is the arrival of the SACW in that area that caused this strong change, and not a surface exchange of freshwater or heat, as showed by Castro (2014) for the central part of the SBB.

Current oscillations at the entrance of the AB are similar to other areas of the SBB. The dominance of the barotropic mode in the AB entrance, especially in the subtidal frequency band, has been seen by several authors in the SBB (Castro and Miranda 1998; Dottori and Castro 2009). The most energetic current oscillations are in the subtidal frequency band at the entrance of the AB, forced by the wind stress oscillations, agreeing with other authors that analyzed other points in the SSC (Emilsson 1962; Kvinge 1967; Castro 1990), and also with papers that examined current measurements at the SBB (Castro and Lee 1995; Dottori and Castro 2009).

The flooding and drying of the AB tidal flat are a consequence of the sea level rise and fall due to tidal oscillations, as usual for tidal flats. Nevertheless, the physical properties and the quality of the water that inundates the AB tidal flat are controlled by subtidal oscillations.

References

Amaral ACZ, Migotto AE, Turra A, Schaeffer-Novelli Y (2010) Araçá: biodiversity, impacts and threats. Biota Neotrop 10(1):219–264

Campos EJ, Velhote D, da Silveira IC (2000) Shelf break upwelling driven by Brazil Current cyclonic meanders. Geophys Res Lett 27(6):751–754

Castro BM (1990) Wind driven currents in the channel of São Sebastião: winter, 1979. In: Braz J Oceanogr 38(2):111–132

Castro BM (1996) Correntes e massas de água da Plataforma Continental Norte de São Paulo. Dissertation (Tese de Livre Docência), Instituto Oceanográfico da Universidade de São Paulo

Castro BM (2014) Summer/winter stratification variability in the central part of the South Brazil Bight. Cont Shelf Res 89:15–23

Castro BM, Lee TN (1995) Wind-forced sea level variability on the southeast Brazilian shelf. J Geophys Res 100(8):16045–16056

Castro BM, Miranda LB, Miyao SY (1987) Condições hidrográficas na plataforma continental ao largo de Ubatuba. Bol Inst Oceanogr, S Paulo 35(2):135–151

Castro BM et al (2008) Processos físicos: hidrografia, circulação e transporte, Oceanografia de um Ecossistema Subtropical: Plataforma de São Sebastião, SP, São Paulo: Editora da Universidade de São Paulo: 59-121

Cerda C, Castro BM (2013) Hydrographic climatology of South Brazil Bight shelf waters between Sao Sebastiao (24° S) and Cabo Sao Tome (22° S). Cont Shelf Res 89:5–14

Clarke AJ, Brink KH (1985) The response of stratified, frictional flow of shelf and slope waters to fluctuating large-scale, low-frequency wind forcing. J Phys Oceanogr 15(4):439–453

Coelho AL (1997) Massas de água e circulação no Canal de São Sebastião (SP). *Massas de água e circulação no Canal de São Sebastião (SP)*. Dissertation (Masters), Instituto Oceanográfico da Universidade de São Paulo

Csanady GT (1977) Intermittent 'full'upwelling in Lake Ontario. J Geophys Res 82(3):397–419

Csanady GT (1978) The arrested topographic wave. J Phys Oceanogr 8(1):47–62

Castro BM, de Miranda LB (1998) Physical oceanography of the western Atlantic continental shelf located between 4 N and 34 S. The Sea 11(1):209–251

Dionne J (1988) Characteristic features of modern tidal flats in cold regions. Tide-Influenced Sedimentary Environments and Facies, Springer, pp 301–332

Dottori M, Castro B (2009) The response of the Sao Paulo Continental Shelf, Brazil, to synoptic winds. In: Ocean Dyn 59(4):603–614

Dyer K, Christie M, Wright E (2000) The classification of intertidal mudflats. In: Cont Shelf Res 20(10):1039–1060

Emilsson I (1961) The shelf and coastal waters of Southern Brazil. Bol Inst Oceanogr 7(2):101–112

Emilsson I (1962) As correntes martimas no Canal de São Sebastião. Ciência e Cultura 14(4):269–270

Gill AE, Schumann EH (1974) The generation of long shelf waves by the wind. J Phys Oceanogr 4(1):83–90

Kanamitsu M, Ebisuzaki W, Woollen J, Yang SK, Hnilo JJ, Fiorino M, Potter GL (2002) NCEP-DOE AMIP-II reanalysis (R-2). Bull Am Meteorol Soc 83(11):1631–1643

Kvinge T (1967) On the special current and water level variations in the Channel of São Sebastião. Bol Inst Oceanogr 16(1):23–38

McClimans TA (1986) Laboratory modeling of dynamic processes in fjords and shelf waters. The Role of Freshwater Outflow in Coastal Marine Ecosystems. Springer, Berlin Heidelberg, pp 67–84

Silva LDS, Miranda LBD, Castro Filho BMD (2005) Numerical study of circulation and thermohaline structure in the São Sebastião Channel. Rev Bras Geof 23(4):407–425

Stech JL, Lorenzzetti JA (1992) The response of the South Brazilian Bight to the passage of wintertime cold fronts. J Geophys Res 97(6):9507–9520

Villamarin BC (2014) Alterações morfológicas da Baia do Araçá: implicações em sua dinâmica, Graduation monography

Welch PD (1967) The use of fast Fourier transform for the estimation of power spectra: a method based on time averaging over short, modified periodograms. IEEE Trans Audio Electroacoust 15(2):70–73